International Journal of Wildland Fire http://dx.doi.org/10.1071/WF14089

Interactions of fires of neighbouring shrubs in two- and three-shrub arrangements

Ambarish Dahale^A, Babak Shotorban^{A,B} and Shankar Mahalingam^A

Abstract. A physics-based computational model was utilised to better understand the interactions of fires generated by burning of neighbouring shrubs. The model included large-eddy simulation for flow field turbulence and a two-phase approach for the coupling of solid fuel and gas phases. Two different arrangements consisting of two and three identical shrubs placed adjacent to each other were considered. All shrubs were simultaneously ignited from their base with the aid of separate ground fuels. Both crown and ground fuels were modelled as porous media with thermophysical properties of chamise and excelsior respectively. Modelling results indicated that the peak mass-loss rate and the vertical fire spread rate within a shrub decrease when the shrub separation distance increases. At zero separation, heat release rate normalised by the number of shrubs is enhanced by 5 and 15% for the two-shrub and the three-shrub arrangements, respectively. Generation of strong vorticity by higher gravitational torque appeared to be the cause for enhanced burning in the three-shrub arrangement. This effect was seen to be much weaker for the two-shrub arrangement. Interactions between the individual fires cease for a centre-to-centre distance of 1.5 and 2 times the shrub diameter for the two-shrub and the three-shrub arrangement respectively.

Additional keywords: physics-based modelling, shrub fires.

Received 23 May 2014, accepted 25 January 2015, published online xx xxxxx xxxx

Introduction

In recent years, important developments have been made through experimental or computational modelling approaches (Weise *et al.* 2005; Zhou *et al.* 2005; Porterie *et al.* 2007; Lozano 2011) to better understand the process of fire spread through vegetation. However, most of these studies considered fire spread through a single shrub (Tachajapong 2008; Mell *et al.* 2009; Dahale *et al.* 2013) or a fuel bed (Porterie *et al.* 2000; Mell *et al.* 2007; Zhou *et al.* 2007) where the interactions between flames generated from neighbouring fuel elements ignited simultaneously are not explicitly considered.

Fire-fire interactions and the subsequently generated mass fires have been a topic of interest in fire research for a long time, not only owing to the peculiar characteristics associated with them but also the varied circumstances under which they are seen (Finney and McAllister 2011). A mass fire is described as a scenario where individual fires interact and exhibit a unified behaviour (Countryman 1964). During a wildfire, interactions between two or more fires with the potential of creating a mass fire are routinely observed (Byram 1954).

While developing a new method for carrying out prescribed burns that involved dropping of ignition sources from air, Rothermel (1984) raised concerns over generation of merged fires. His analysis suggested that when two initially separated fires approach each other, thermal energy is accumulated between them, resulting in intense heating and subsequent faster combustion of the fuel in this region. Accelerated burning can lead to higher flame heights and in some cases leads to the torching of tree crowns, if present. Occurrence of merging phenomena is considered hazardous, as it may cause the prescribed fires to go out of control. Baum and McCaffrey (1989) studied the flow field induced by pool fires ranging over four orders of magnitude in size, through theory and experimentation. They concluded that the velocity of the horizontally induced draft, even though lower when compared with those observed in the plume for isolated fires, can exceed the net vertical plume velocity in presence of large numbers of surrounding fires.

Baldwin *et al.* (1964) conducted experimental investigation on fire-merging using two and four gas burners placed side by side and burning at constant rates. Further, they proposed a theoretical model correlating the buoyancy force and the pressure thrust due to external wind with the amount of tilt each flame experiences. Modelling assumptions included flame temperature remaining constant throughout its volume, negligible viscous forces and constant external wind velocity. The model predictions and experimental results showed considerable difference when the fires were too close or too far apart. These differences were attributed to the lack of robustness of the model as well as the uncertainties involved in experiments.

^ADepartment of Mechanical and Aerospace Engineering, University of Alabama in Huntsville, AL 35899, USA.

^BCorresponding author. Email: babak.shotorban@uah.edu

B Int. J. Wildland Fire A. Dahale et al.

Recently, several researchers have performed computational and experimental studies with propane burners arranged in square arrays to analyse the effects of flame merging on overall fire behaviour (Fukuda et al. 2004; Weng et al. 2004; Kamikawa et al. 2005). A dimensionless heat release rate and flame height were introduced to identify the effects of flame merging. They observed that the flame height of merged fire is substantially larger than that of an individual fire burning under identical conditions. For example, the height of a merged flame from a 4×4 configuration of square propane burners was reported to be almost twice that observed in an isolated fire (Fukuda et al. 2004). They also found that the flame height is larger for a larger array of fires. They showed that flame merging did not occur for fires with heat release rate smaller than a critical value and this critical heat release rate varied with the number of surrounding fire sources as well as the separation between them.

Satoh et al. (2007) conducted computational modelling and experimentation on pool fires generated from circular pans filled with liquid fuel and arranged in square arrays. They considered large arrays, e.g. 19×19 , to increase the overall surface area of fire and performed simulations by modelling the combustion process as constant heat release rates over the base areas of the pool fires. Visual observation was used as a criterion in experiments to identify flame merging, whereas thermal iso-surfaces of 313°C were used to identify flame merging from simulation results. The critical merging distance, i.e. the largest distance between two fires where flame merging is observed, was reported to increase with an increase in heat release rates of individual pool fires. Later, Satoh et al. (2011) conducted a computational fluid dynamics (CFD) based analysis on flame interactions from oil depot fires and observed the creation of a negative pressure zone at the centre of the merged fire. They concluded that this negative pressure is the cause of larger horizontal indrafts of ambient air, which in turn are the reason for the increase in the overall flame height.

Morvan *et al.* (2011, 2013) studied the interactions between two fire fronts (a head fire and a back fire) that propagate through a fuel bed, using a physics-based model. The motivation behind this research was from a firefighting standpoint, where a back fire is used to eliminate the fuel ahead of the main propagating fire front. Total heat release rate from the fires was used as a criterion to identify the onset of flame-merging phenomena. They observed that when the two fire fronts are in close proximity, the back fire is pulled towards the head fire by induced drafts. Furthermore, they observed that flame merging leads to a considerable increase in total heat release rate, and concluded that the buoyancy-driven flow field generated by the head fire acts as a screen, shielding the effects of external wind on the back fire.

In the present paper, the focus is on gaining a better understanding of interactions between fires generated by neighbouring shrubs. Two different kinds of shrub arrangements are considered: a two-shrub arrangement and a three-shrub arrangement. In the former, the shrubs are placed adjacent to each other and in the latter, the shrubs are placed on the vertices of an equilateral triangle. An additional configuration with only a single shrub is also modelled for comparison purposes. In all three configurations, the modelled shrubs are identical to each other, with thermophysical properties of chamise (*Adenostoma fasciculatum*)

and a fixed bulk density of 3.8 kg m⁻³ throughout the canopy volume (Dahale *et al.* 2013). It is noted that the presence of external wind, depending on its direction and velocity, can substantially change the behaviour of fires (Albini 1981). External wind results in effects such as tilting of the flame, increasing the fire spread rate (Nelson *et al.* 2012) and generating fire whirls (Pitts 1991) that can complicate the analysis of flame-merging. The focus here is on analysing shrub fire merging in a quiescent environment, i.e. with no external wind. The approach adopted for conducting the present study is physics-based modelling, wherein governing equations for various significant physical phenomena involved in the fire are solved numerically. The next section provides a brief description of the mathematical model used.

Modelling setup and approaches

Fig. 1a is a schematic of the computational domain in which the shrub arrangement and the ignition zone adopted for the modelling of a single-shrub case is shown. The size of the computational domain in the x, y and z directions is 4.0, 6.0 and 4.0 m respectively, with the ignition zone and crown fuel located at the centre. The dimensions of the ignition zone are 0.2, 0.1 and 0.2 m in the x, y and z directions respectively. The single-shrub arrangement is motivated by experimental results reported by Li (2011) and previous single-shrub modelling results that we reported in Dahale et al. (2013). The two- and the three-shrub arrangements that were chosen to study the interactions of shrub fires are shown in Fig. 1b and Fig. 1c respectively. The line contour in these figures represents the solid fuel bulk density on an xz-slice passing through y = 1 m (top view of the computational domain), where d is the distance between edges of the shrubs and D is the largest diameter of the shrub along its vertical axis. Each shrub has an individual ignition zone located below the crown fuel similar to the one shown in Fig. 1a.

Two types of solid fuel with identical moisture content are considered in the shrub to model the foliage and branches. In our previous work (Dahale et al. 2013), we studied the effect of fuel moisture content (FMC) on the burning of a single shrub and found that as FMC increases, the shrubs burn slowly, generating smaller flame heights. This in turn reduces the velocity of the induced draft. For this reason, the moisture content of all the modelled shrubs is set to a small value of 10% to lead to an appreciable flame interaction. The unburned mass of each shrub is \sim 0.6 kg and its bulk density is 3.8 kg m⁻³, assumed constant throughout its volume. For additional details on the dimensions and physical properties of the shrub, readers are referred to Dahale et al. (2013) and Dahale (2014). As excelsior is typically used as ground fuel during burn experiments, the ignition zone is modelled with properties of excelsior with a moisture content of 7% (Tachajapong 2008). To ignite the solid fuel, a volumetric heating source is used, which is active only in the ignition zone. During ignition, the heating of the solid fuel is modelled through the mechanism of convective heat transfer. The external heat source is terminated when 80% of the fuel in the ignition zone is consumed. This ignition mechanism is akin to ignition caused by spotting phenomena, commonly seen during intense wildfires (Li 2011). Nevertheless, the effect of an external ignition mechanism on the simulation results is assumed negligible

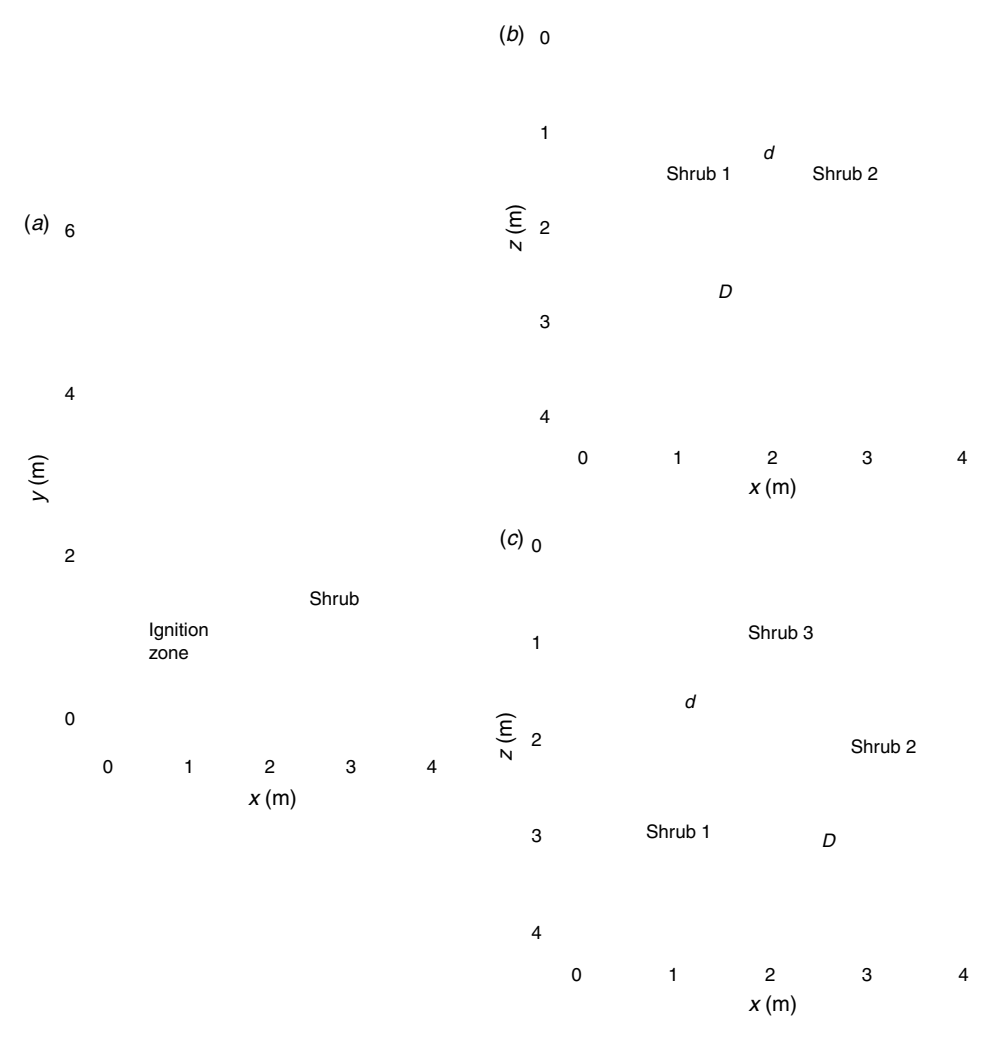


Fig. 1. (a) A front view of the computational domain in the single-shrub case; top view of the computational domain showing generic arrangement for (b) the two-shrub cases, and (c) the three-shrub cases.

because the igniter is switched off fairly early for all simulations to be discussed here.

Overall, nine cases with different crown separation distances were modelled for the two- and three-shrub configurations. The crown separation distance is defined as the distance between the inner edges of the shrubs (d) normalised by the maximum value of shrub diameter (D) along its height. For the two-shrub configuration, four different values of 0.0, 0.1, 0.3 and 0.5, and for the three-shrub configuration, five different values of 0.0, 0.1, 0.3, 0.5 and 1.0 were considered for d/D. An additional case with a single shrub is also modelled to serve as a baseline. Results obtained from the burning of two and three shrubs are compared against those obtained from the burning of a single shrub to explore the effects of neighbouring fires on the burning of individual shrubs.

A previously developed physics-based model was utilised to carry out the modelling in this work. Details of the model are given by Dahale (2014), with only a brief summary given here: large-eddy simulation (LES) is utilised to deal with the turbulent flow field generated by burning of the solid fuel. The transport

equations in the gas phase are the spatially filtered conservation equations for mass, momentum, energy and species. In addition, a state equation for a multicomponent ideal gas is used. The subgrid-scale (SGS) stresses in the filtered momentum equation are modelled by a dynamic Smagorinsky model, and the SGS energy and species fluxes are modelled by a gradient diffusion model (Pitsch and Steiner 2000). The gas-phase equations also include source terms to capture the influence of the solid phase on the gas phase: conversion of solid mass into gas modelled in the gas-phase continuity equation, the backway effect of drag forces by gas on the solid fuel modelled in the momentum equations, energy transfer by convection and radiation between solid and gas modelled in the energy equation, and decomposition of solid into various gas-phase species modelled in the species transport equations. A flame surface density (FSD) concept is used to model the gas-phase combustion where the reaction is modelled using a global single-step mechanism. Thermal radiation is modelled by a radiation transport equation (RTE) for multiphase, emitting, absorbing and non-scattering media. The gas-phase absorption coefficient is modelled based D Int. J. Wildland Fire A. Dahale et al.

on a grey-gas assumption. Soot transport is modelled via a transport equation for soot volume fraction that includes terms to capture effects of production, oxidation and thermophoretic diffusion of soot. Solid fuel is modelled as a porous medium and, for simplicity, is assumed fixed in space throughout the burning process. The equations for the time evolution of solid-fuel mass account for degradation of solid into water vapour, pyrolysis gases and char. Similarly, the solid-phase energy equation, based on the thermally thin solid particle assumption, includes the effects of energy transfer by convection, radiation and phase change.

The governing equations are discretised on staggered uniform grids through a finite volume method with a resolution of $200 \times 300 \times 200$ in x, y and z directions respectively. The size of the computational domain and the grid resolution used in this work are guided by previous experience with modelling of a single shrub in Dahale et al. (2013). The lateral boundaries of the computational domain are modelled with a pressure-based inlet boundary condition that allows mass flux to freely enter and exit the computational domain. Here, outflow of combustion-generated gases is calculated by setting boundary normal gradients to zero and inflow of ambient air is calculated assuming the fluid is accelerated from stagnation condition in the ambient owing to pressure inside the domain (McGrattan et al. 2007). The top boundary is modelled with a convective outflow boundary condition (Boersma et al. 1998) where the convective velocity is taken to be the local boundary normal velocity. The bottom boundary is modelled with a free slip wall boundary condition so that no mass enters or exits across this boundary. The simulations were performed using message-passing interface (MPI) protocol on 40 processors of the High Performance Technical Computing (HPTC) cluster located at The University of Alabama in Huntsville. A typical simulation representing 70 s of burning required a wall time of ~340 h and 28 GB of memory.

Results and discussion

Zero separation distance

The results of all multishrub fire cases shown in this subsection were obtained for d/D = 0. Fig. 2 shows the flames indicated by the pyrolysis gas mass fraction iso-surface of 0.025 (\sim 5% of maximum) along with a bulk density iso-surface of 3.8 kg m⁻³ used to indicate the solid fuel. It can be seen that a low-intensity flame is established inside the shrubs at $t \approx 16$ s, ~ 6 s after the igniter is turned off. Until this time, no significant interactions are seen between the flames for the two-shrub case whereas some flame-merging phenomena can be seen for the three-shrub case. At time $t \approx 23$ s, when the peak mass-loss rate is reached, the multiple shrubs appear to be a single source of fire, as seen in Fig. 2e and Fig. 2h. Towards the end of the simulation at $t \approx 45$ s, the individual flames are again separated in the twoshrub case, as can be seen in Fig. 2f, whereas the individual flames seem to be still merged in the three-shrub case, as can be seen in Fig. 2i.

The buoyancy-driven flow field generated by the shrub fires is shown in Fig. 3, using a vorticity magnitude iso-surface of 35 s⁻¹ (\sim 25% of maximum). Superimposed on this iso-surface is the colour contour of the second invariant of the velocity gradient tensor Q, often used as a criterion for vortex

identification (Hunt *et al.* 1988). For a velocity field u_i , $\mathcal{Q} = \left(||\Omega||^2 - ||S||^2\right)/2$, where Ω is the rotation rate tensor defined by $\Omega_{ij} = (\partial u_i/\partial x_j - \partial u_j/\partial x_i)/2$, and S is the strain rate tensor defined as $S_{ij} = (\partial u_i/\partial x_j + \partial u_j/\partial x_i)/2$. Thus, positive values of \mathcal{Q} identify regions in the flow field where rotation dominates strain and negative values indicate the reverse. The plumes generated by the three-shrub case display higher magnitudes of both vorticity and strain as compared with those generated by the two-shrub and single-shrub cases, which can be seen by comparing the snapshots from Fig. 3 at corresponding time instances. Possible reasons for the higher vorticity magnitudes in the three-shrub case are discussed later in this section.

The time evolution of the mass of a shrub and its rate of change are shown in Fig. 4. As seen in Fig. 4a, the difference between different cases is negligible at times less than 20 s, indicating minimal flame interactions in either two- or threeshrub arrangements. At later times, from 20 s on, the shrub mass for the three-shrub case is consumed more rapidly than that for two other cases. This observation can be also made in Fig. 4b. The peak value of the mass-loss rate displayed in this figure is largest for the three-shrub case and smallest for the single-shrub case. Owing to the rapid decomposition of the solid fuel, higher amounts of pyrolysis gases are generated, resulting in flames, as seen in Fig. 2h for the three-shrub configuration (at peak massloss rate, $t \approx 23$ s), larger than those of two- and single-shrub cases, as displayed in Fig. 2e and Fig. 2b respectively. The resulting plumes generated by the buoyancy effects appear to be stronger and drawn towards the centre of the domain for the three-shrub configuration, as seen in Fig. 3h, indicating the presence of stronger indrafts of ambient air.

Fig. 5 shows the time history of the total heat release rate per shrub in the domain. This rate is computed from the source term associated with chemical reactions in the gas-phase energy balance equation, i.e. $\Delta V \sum_{K=1}^{N_K} \dot{\omega}_K \Delta h_{f,K}^0$, where $\dot{\omega}_K$ is the production rate for the Kth gas-phase species, $\Delta h_{f,K}^0$ is the enthalpy of formation for the Kth gas-phase species, N_K is the total number of gas-phase species and ΔV is the volume of a computational grid cell. Because in the two-shrub and three-shrub cases more fuel is burned, the total heat released in these cases is larger than that in the single-shrub case. For this reason, the total heat release rate is normalised by the number of shrubs, recalling that all the shrubs are identical and ignited under the same conditions.

During fire propagation, the mass of the solid fuel decreases initially owing to dehydration, then owing to the release of pyrolysis gases and lastly owing to combustion of char. According to the shape of shrub adopted in this study (for more details on shrub geometry, refer to Dahale $et\ al.\ 2013$), the mass of the shrub per unit height increases as we move from the bottom towards the top surface. Therefore, at some point during the burning process, if a large volume of shrub is undergoing dehydration, its mass will decrease, but because only water vapour is being released, the amount of heat generated from gasphase combustion will decrease. Once dehydration is completed, pyrolysis starts, which increases the heat release rate. This phenomenon can lead to the two peaks seen in the heat release rate curve (Fig. 5) as opposed to a single peak seen in the massloss rate curve (Fig. 4b).

Е

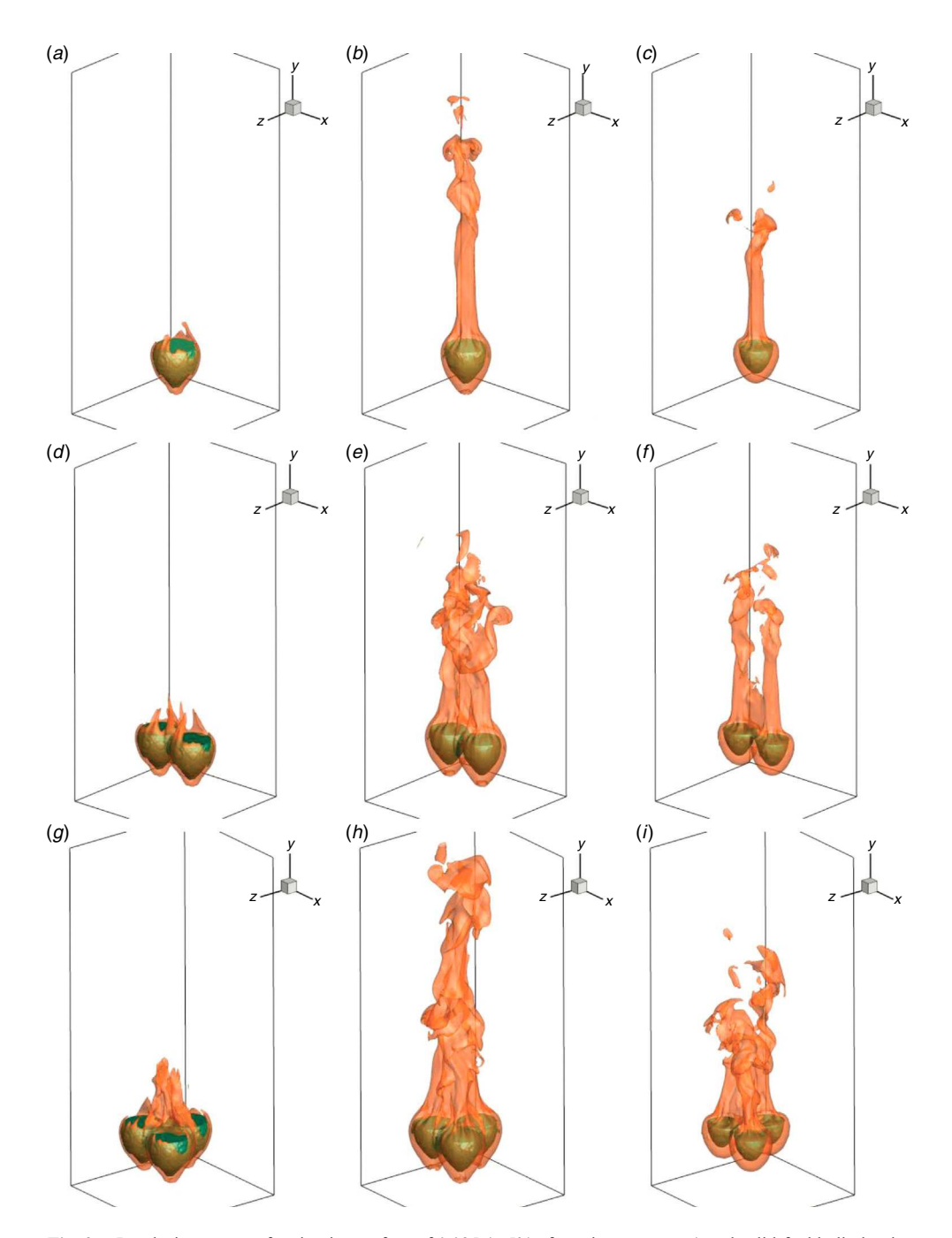


Fig. 2. Pyrolysis gas mass fraction iso-surface of 0.025 (\sim 5% of maximum, orange) and solid-fuel bulk density iso-surface of 3.8 kg m⁻³ (green) at t = 16 s (first column), t = 23 s (second column) and t = 45 s (third column) in single-shrub (a–c), two-shrub (d–f), and three-shrub (g–i) cases; d/D = 0 in all cases.

It is seen in Fig. 5 that the heat release per shrub in the three-shrub case is substantially larger than that in the two-shrub and single-shrub cases. Within the same time interval, the heat release per shrub for the two-shrub case is higher than the single-shrub case. This effect highlights the occurrence of the flame-merging phenomenon where the heat released from the merged flame is higher than the heat released from the individual flames combined. A similar observation was made by Morvan *et al.* (2013) who studied fire propagation through

grasslands, where a spike in the heat release rate was reported at the time of flame merging between a head and a back fire.

Fig. 6 depicts instantaneous snapshots of the gas-phase temperature in an xy-slice passing through the centre of the computational domain (i.e. z=2 m) at the time of peak massloss rate ($t \approx 23$ s). The flame height indicated by the gas-phase temperature iso-contour of 500 K is observed to be considerably larger for the three-shrub case, as displayed in Fig. 6c, than for the single- and the two-shrub cases, as displayed in Fig. 6a, b

Int. J. Wildland Fire
A. Dahale et al.

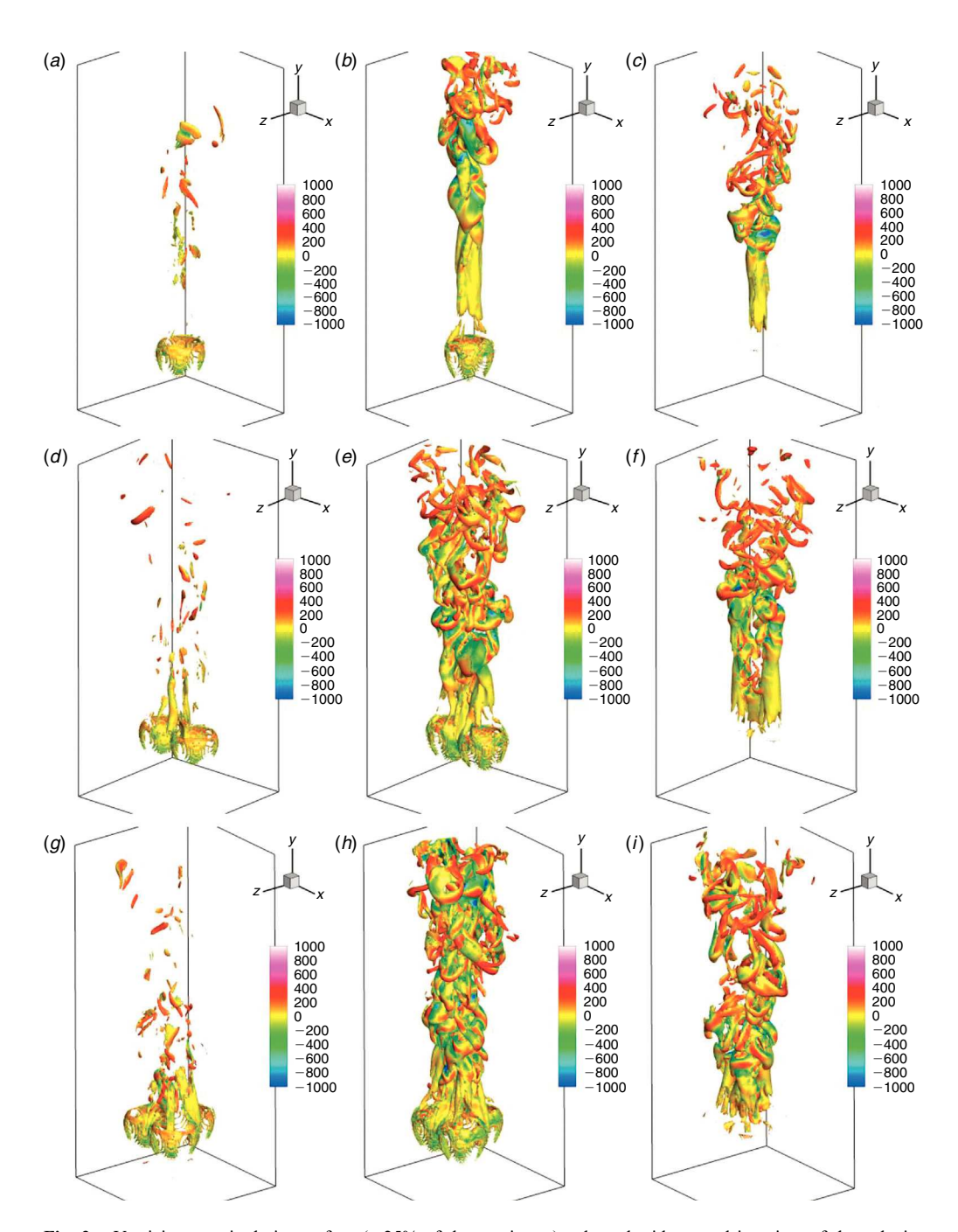


Fig. 3. Vorticity magnitude iso-surface (\sim 25% of the maximum) coloured with second invariant of the velocity gradient tensor Q at t=16 s (first column), t=23 s (second column) and t=45 s (third column) in single-shrub (a–c), two-shrub (d–f), and three-shrub (g–i) cases; d/D=0 in all cases.

respectively. By analysing the temperature snapshots at different time instances, the gas-phase temperature in the three-shrub case is found to be higher than that in the single- and the two-shrub cases.

The strength of the generated plume is studied by examining the total kinetic energy given by $\frac{1}{2}(\tilde{u}^2 + \tilde{v}^2 + \tilde{w}^2)$, where \tilde{u} , \tilde{v} , and \tilde{w} are the Favre filtered velocity components obtained through LES in x, y and z directions respectively. Fig. 7 shows contours of the total kinetic energy in an xy-slice passing

through the centre of the computational domain. The snapshots shown are at the time of the peak mass-loss rate, which is $t \approx 23$ s. The kinetic energy of the plume for the three-shrub case is observed to be much higher as compared with that in the single- and two-shrub cases. This observation indicates that the ambient air is displaced at higher velocity, resulting in a stronger plume for the three-shrub case.

In order to better quantify the difference between the fire interactions in the two- and three-shrub cases, gas-phase

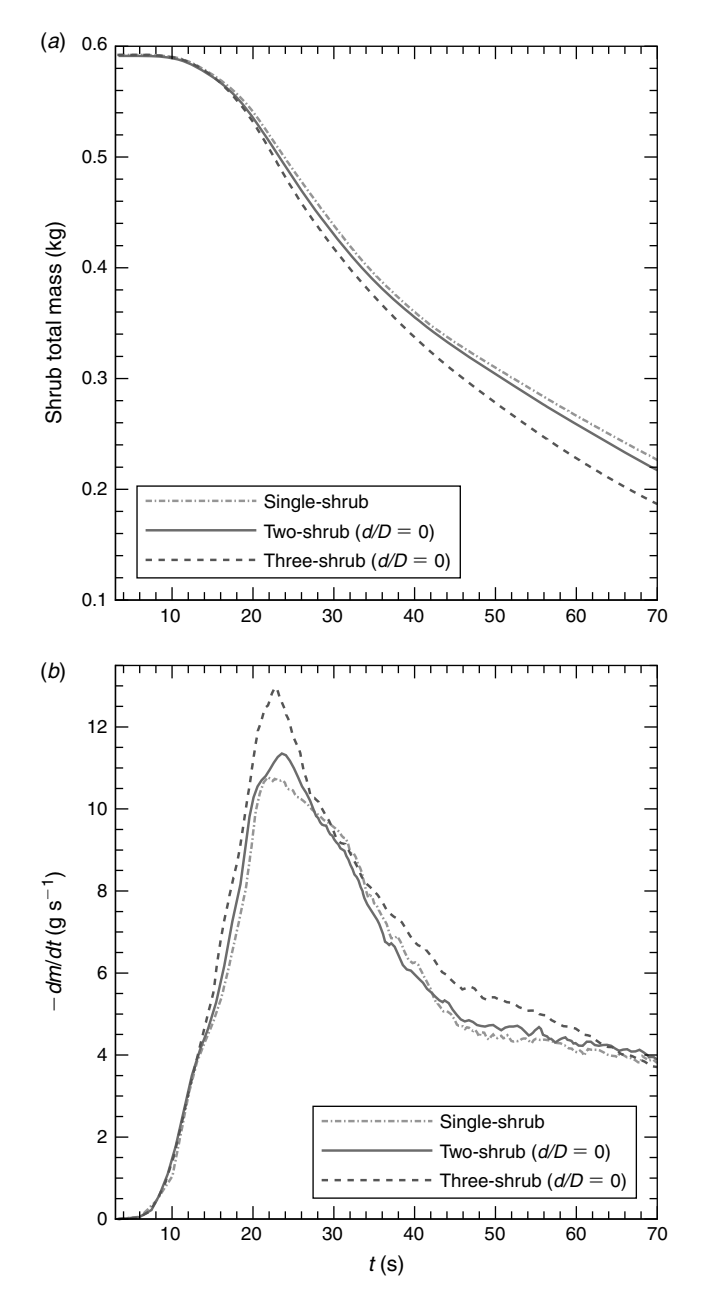


Fig. 4. Time evolution of (a) mass of a shrub in kilograms; and (b) massloss rate of shrub in grams per second for single-, two- (d/D = 0), and three-shrub (d/D = 0) cases.

variables are plotted against y along the centreline of the domain, in Fig. 8, at the time when the mass-loss rate is maximum. Panels (a), (b) and (c) are for the gas-phase temperature, total kinetic energy and relative pressure respectively. It is evident that the kinetic energy is substantially larger and the pressure is significantly more negative in the three-shrub case. Higher gas-phase temperatures are seen for the three-shrub arrangement mostly in the plume region. By analysing velocity components, it is seen that the velocity component along the vertical direction y for the three-shrub case is much higher than that for the single- and two-shrub cases. The presence of a strong updraft in the three-shrub case, driven by conservation of mass,

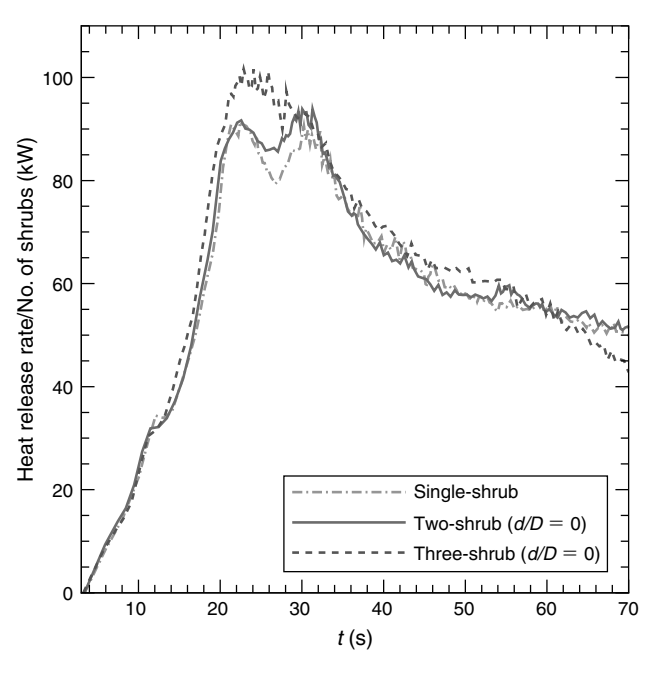


Fig. 5. Time evolution of the heat release rate (kW) per shrub for single-, two- (d/D=0), and three-shrub (d/D=0) cases.

results in larger cross-stream velocities (in x and z directions) in regions near the shrub or the base of the plume. These strong indrafts further enhance the burning of the solid fuel, leading to the generation of intense vorticity in the core, central region surrounded by the three shrubs.

The vorticity transport Eqn 1, obtained by applying the curl operator to the momentum transport equation, contains source and transfer terms such as baroclinic torque, gravitational torque, vorticity modification by volumetric expansion and vortex stretching (DesJardin *et al.* 2004).

$$\frac{D\omega}{Dt} = \underbrace{(\omega \cdot \nabla)\mathbf{V}}_{\text{vortex streching}} - \underbrace{\omega(\nabla \cdot \mathbf{V})}_{\text{dilatation}} + \underbrace{\frac{1}{\rho^2}(\nabla \rho \times \nabla p)}_{\text{baroclinic torque}} + \underbrace{\frac{\rho_{\infty}}{\rho^2}(\nabla \rho \times \mathbf{g})}_{\text{gravitational torque}} + \underbrace{\nabla \times \left(\frac{\nabla \cdot \tau}{\rho}\right)}_{\text{viscous torque}}$$
(1)

where ω is the vorticity vector, V is the velocity vector, ρ is density, ρ_{∞} is density at far field and τ is viscous stress. The baroclinic torque, which represents the interaction between density gradient and pressure gradient, and the gravitational torque, which represents the interaction between density gradient and gravitational acceleration, contribute to the generation of vorticity (Ghoniem et al. 1996). Recent studies on buoyancy-driven plumes have shown that the gravitational torque is the dominant factor for vorticity generation at the plume source (DesJardin et al. 2004), arising owing to misalignment between the density gradient vector and the gravitational acceleration vector.

Fig. 9 shows the magnitude of the gravitational torque (colour contours), vorticity (vector field) and the solid-fuel

Int. J. Wildland Fire

A. Dahale et al.

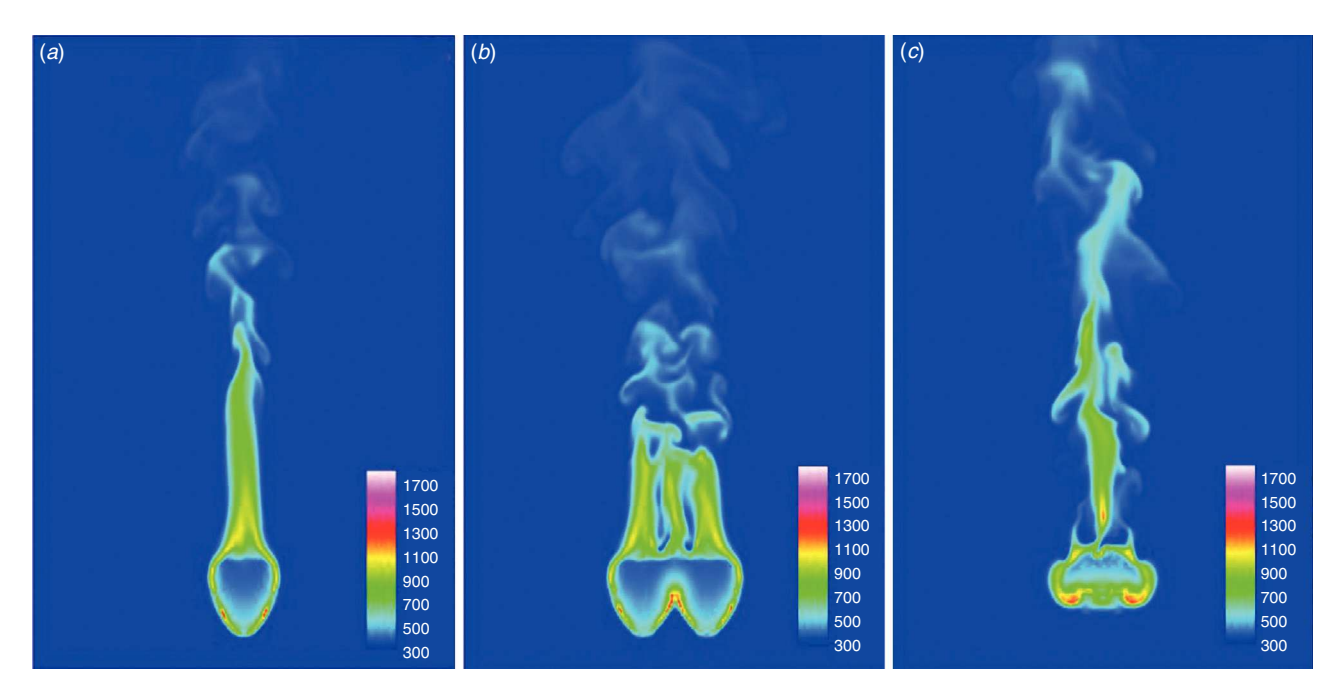


Fig. 6. Gas-phase temperature in Kelvin (colour contours) along an xz-slice at z = 2 m at $t = 23 \pm 0.5$ s (at approximately the time of peak mass-loss rate); (a) single-, (b) two- (d/D = 0), and (c) three-shrub (d/D = 0) cases respectively.

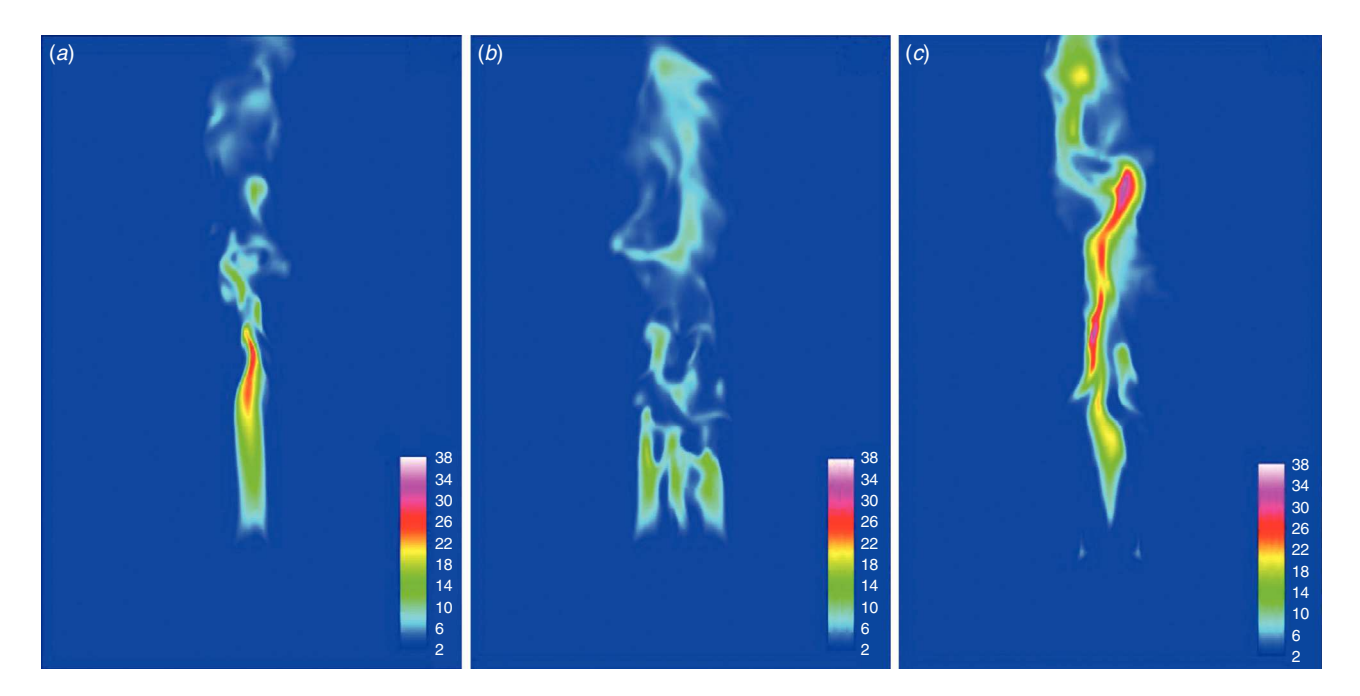


Fig. 7. Contours of kinetic energy (m^2 s⁻²) on an xz-slice at z = 2 m at $t = 23 \pm 0.5$ s (approximately at the time of peak mass-loss rate); (a) single-, (b) two- (d/D = 0), and (c) three-shrub (d/D = 0) cases respectively.

bulk density (line contour) in an xz-plane passing through the top surface of the shrubs located at y=1 m at the time of the peak mass-loss rate. The magnitudes of the gravitational torque in the zone between the shrubs in the three-shrub case, seen in Fig. 9c, are higher than those in the single- and two-shrub cases, seen in Fig. 9a and b respectively. Magnitudes of baroclinic torque, not shown here, are also larger in the three-shrub case.

Η

Higher magnitudes of these two source terms contribute to the generation of intense vorticity in the three-shrub case. This highly rotational flow augments mixing between the pyrolysis gases and the ambient air for the three-shrub case and to some extent for the two-shrub case, resulting in enhanced combustion as well as amplification of interactions between the individual plumes.

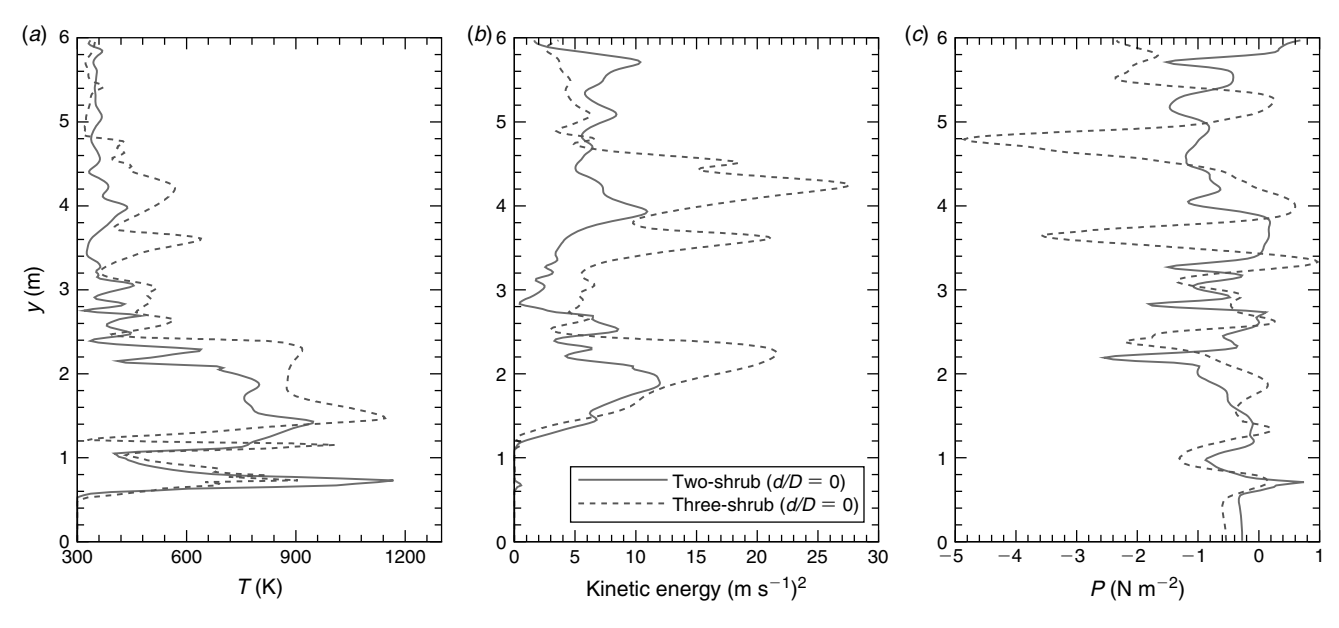


Fig. 8. Spatial variation of (a) gas-phase temperature; (b) kinetic energy; and (c) pressure, along a line passing through the centre of the domain (x = 2.0 m, z = 2.0 m) in y direction at $t = 23 \pm 0.5 \text{ s}$ (at approximately the time of the peak mass-loss rate).

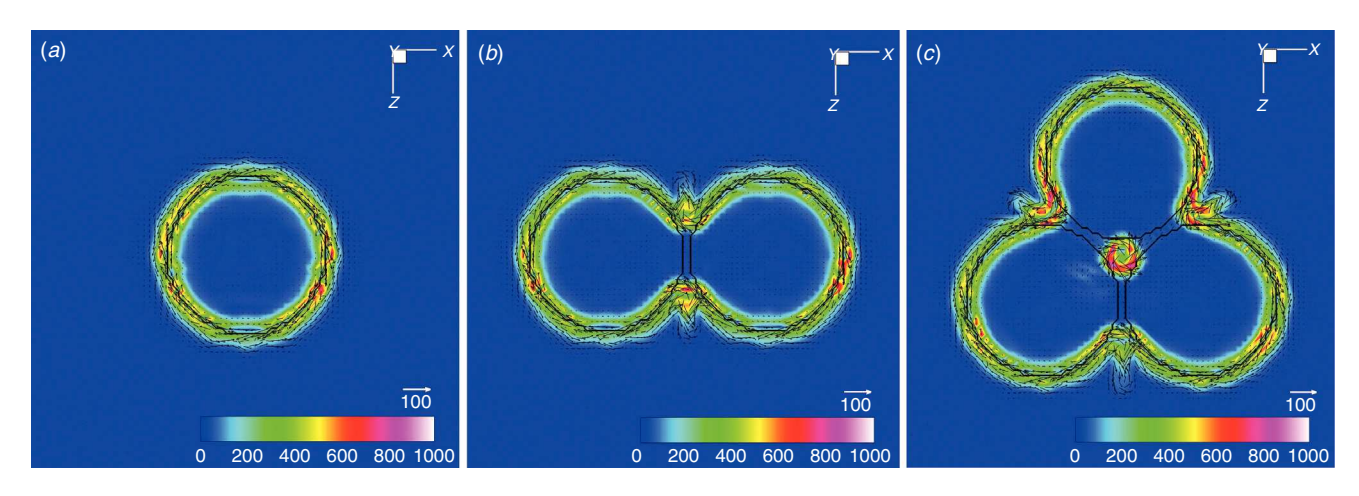


Fig. 9. Colour contours of gravitational torque magnitude (s^{-2}) (see Eqn 2), vectors of vorticity (s^{-1}), and a line contour of solid fuel bulk density of 3.8 kg m⁻³ on an *xz*-slice at y = 1 m, at $t = 23 \pm 0.5$ s (at approximately the time of the peak mass-loss rate); (a) single-, (b) two- (d/D = 0), and (c) three-shrub (d/D = 0) cases respectively.

To investigate the effect of the flame-merging phenomena on solid fuel combustion, various terms present in the solid-phase energy balance equation, written as:

$$\frac{d(c_p m T_s)}{dt} = q_{\text{conv}} + q_{\text{rad}} + q_{\text{mass}}$$
 (2)

are considered (Dahale *et al.* 2013). In Eqn 2, T_s , m and c_p are the temperature, mass and specific heat of the solid phase respectively. The three source terms (q) on the right-hand side of Eqn 2 indicate convective heating, radiative heating and heat transfer required for phase change respectively. Fig. 10 shows the

instantaneous snapshots at the time of the peak mass-loss rate for the solid-phase temperature (first-row panels), convective heat transfer between solid and gas phase (second-row panels), and radiative heat transfer between solid and gas phase (third-row panels). The contours are displayed in an xz-slice passing through y=0.71 m, which is approximately the location of the pyrolysis front at the time of peak mass-loss rate. The pyrolysis front is defined based on the average solid-phase temperature of 500 K, where averaging is performed on horizontal (xz) shrub surfaces (Dahale z0. 2013). Higher solid-phase temperatures are seen in regions close to the interaction zone, i.e. the centre of the domain, for the three-shrub case, compared with that in the

J Int. J. Wildland Fire A. Dahale et al.

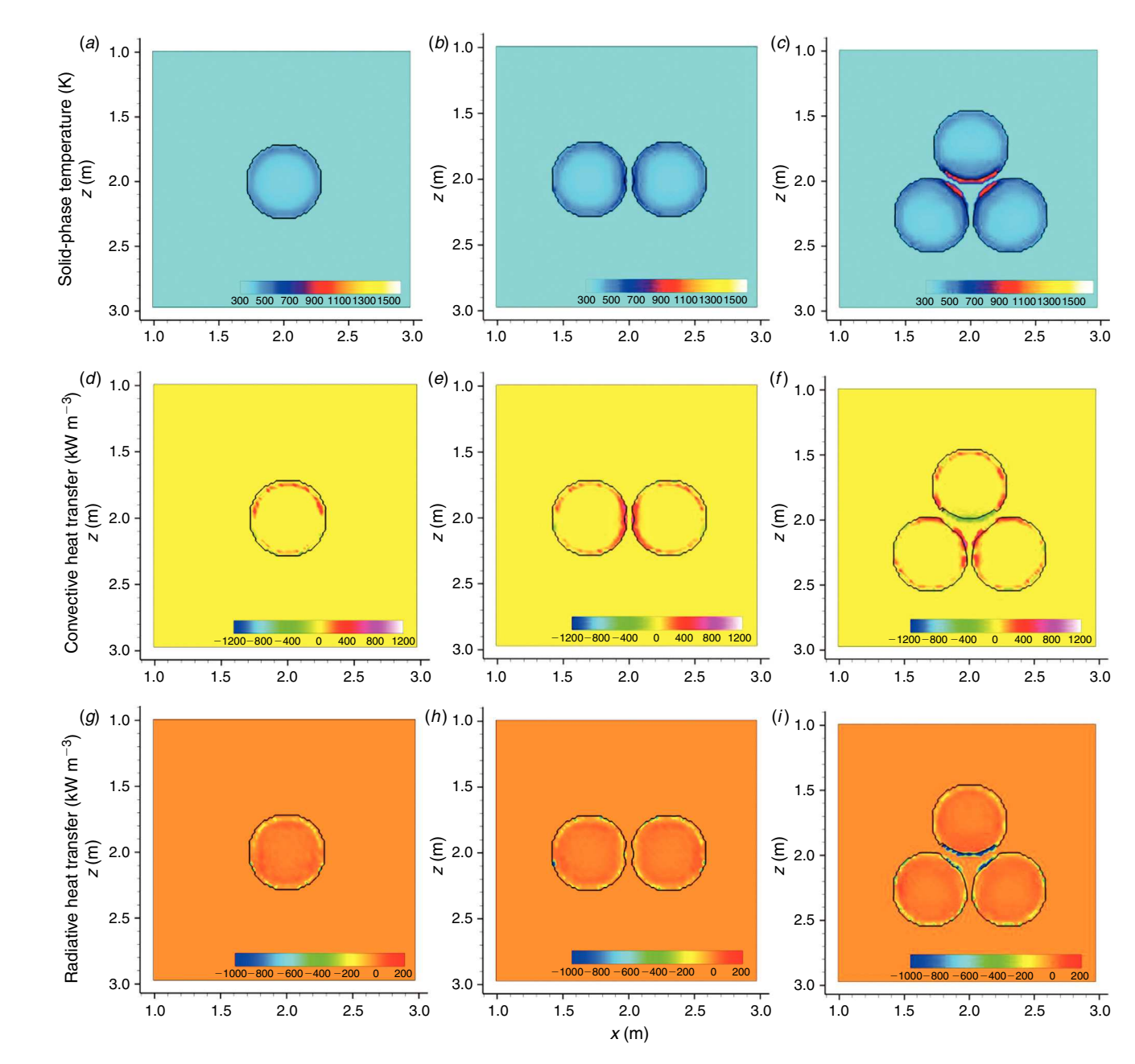


Fig. 10. Solid-phase temperature in Kelvin (a-c), convective heat transfer between the solid and gas phases (kW m⁻³) (d-f), and radiative heat transfer between the solid and gas phases (kW m⁻³) (g-i) along an xz-slice at y=0.71 m at the time of the peak mass-loss rate $(t=23\pm0.5 \text{ s})$ for single-(first column), two- (second column), and three-shrub (third column) cases respectively; d/D=0 for two- and three-shrub arrangement cases.

single- and two-shrub cases. This observation indicates a stronger feedback mechanism of energy from the combustion of pyrolysis gases in the gas phase to the solid phase. Two important modes of heat exchange between the gas and solid phases, which are responsible for the fire spread, are convection and radiation heat transfer (Anderson 1969). For the two-shrub case, the convective heat transfer rates in the solid fuel near the interaction zone, where the two shrubs touch each other, as seen in Fig. 10e, are larger than those for the single-shrub case. The convective heat transfer between the gas and solid phase is

further enhanced for the three-shrub case, as seen in Fig. 10f, especially in regions close to the interaction zone. Negative values of convective heat transfer are seen in the three-shrub case, which demonstrates that the solid-phase temperature is higher than the gas-phase temperature. Mostly negative values are seen for the radiative term, as displayed in the third-row panels of Fig. 10, indicating that heat is being transferred from solid to gas phase. This observation shows that the heating of the solid phase is mainly convection dominant. This observation agrees well with the findings from the previous study on single

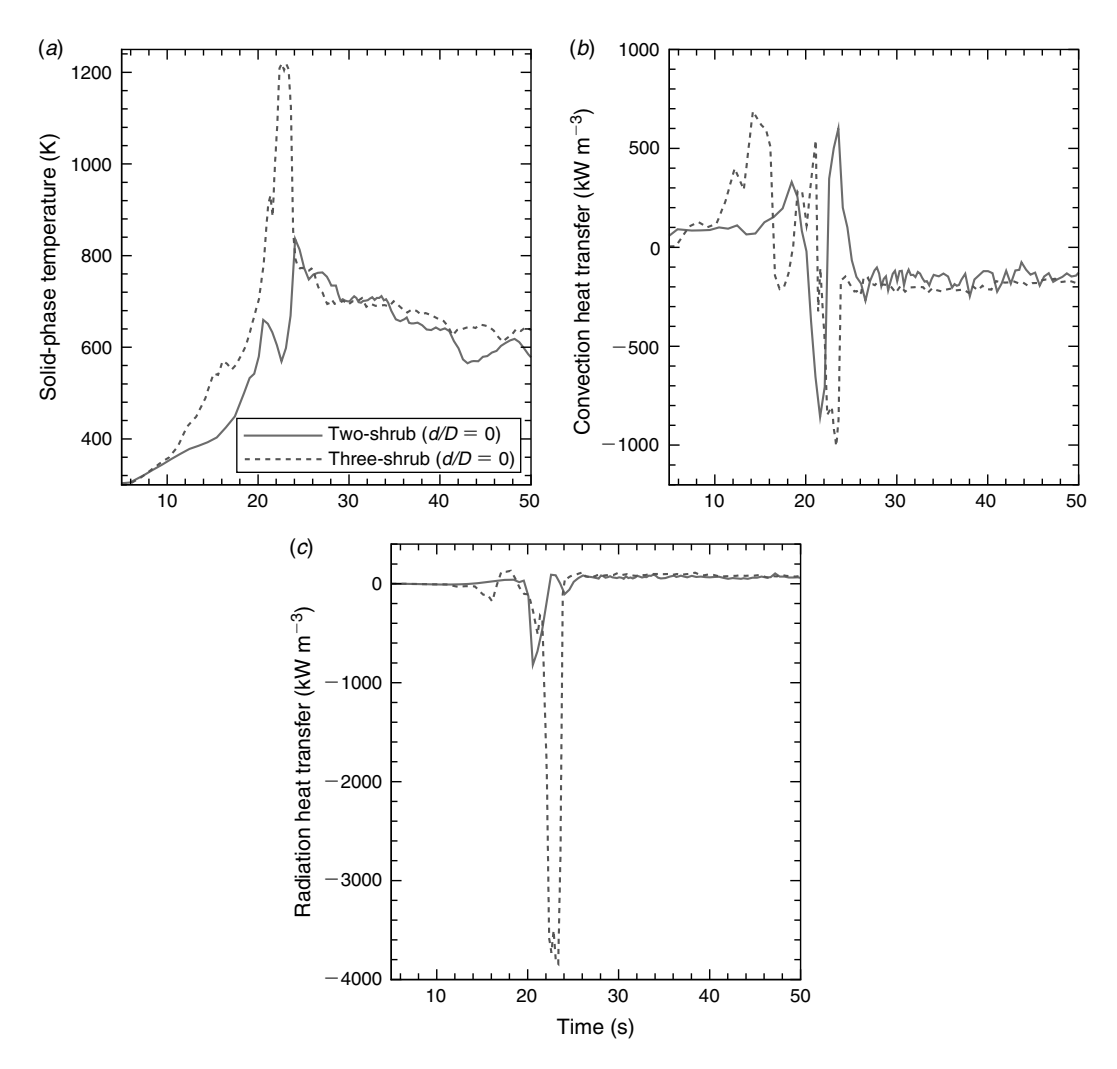


Fig. 11. Time evolution of (a) solid-phase temperature in Kelvin, (b) convective heat transfer between the gas and solid phases (kW m⁻³), and (c) radiative heat transfer between the gas and solid phases (kW m⁻³). Data extracted from a single point located at x = 1.93 m, y = 0.71 m, z = 1.99 m for the two-shrub case (d/D = 0) and x = 1.97 m, y = 0.71 m, z = 2.01 m for the three-shrub case (d/D = 0).

isolated shrub fires (Dahale *et al.* 2013), where convective heating was mainly responsible for vertical fire spread through the shrub.

The temporal evolution of solid fuel variables at various locations were analysed to identify the effect of the convective and the radiative heating mechanisms on the solid fuel temperature. Fig. 11 shows the time history of the solid-phase temperature, convective heat transfer and radiative heat transfer rates for the two- and three-shrub cases at a point located near the interaction zone. As the crown fuels are ignited at their respective bottom surfaces, the fire spreads vertically along the *y* direction within the shrub. For this reason, the two point locations used in Fig. 11 were chosen to have the same vertical distance from the ground in the two-shrub and three-shrub cases. The solid fuel for the three-shrub case shows faster heating compared with that for the two-shrub case (Fig. 11b). Because of this, in the three-shrub case, temperature rises rapidly, as can be

seen in Fig. 11a. This observation indicates that the fire spreads faster within the shrub for the three-shrub case than that for the two-shrub case. Furthermore, significantly higher solid-phase temperatures are experienced in the three-shrub arrangement. It is seen in Fig. 11c that the radiative heat is mainly transferred from the solid to the gas phase and its magnitude is much higher for the three-shrub arrangement.

In wildfire modelling, a solid-phase temperature of 500 K is often used to track the location of the pyrolysis front (Morvan and Dupuy 2004; Porterie *et al.* 2000). Fig. 12*a* shows the time required by the horizontal shrub surfaces (xz planes) to reach an average temperature of 500 K. This time is denoted by t_{500} . Because statistical homogeneity is lacking in any spatial direction, averaging of the solid-phase temperature is performed on horizontal surfaces (xz planes) at various y locations along the vertical direction. The fire spread rate is thus computed by taking a derivative of the position versus time curve of the

L Int. J. Wildland Fire A. Dahale et al.

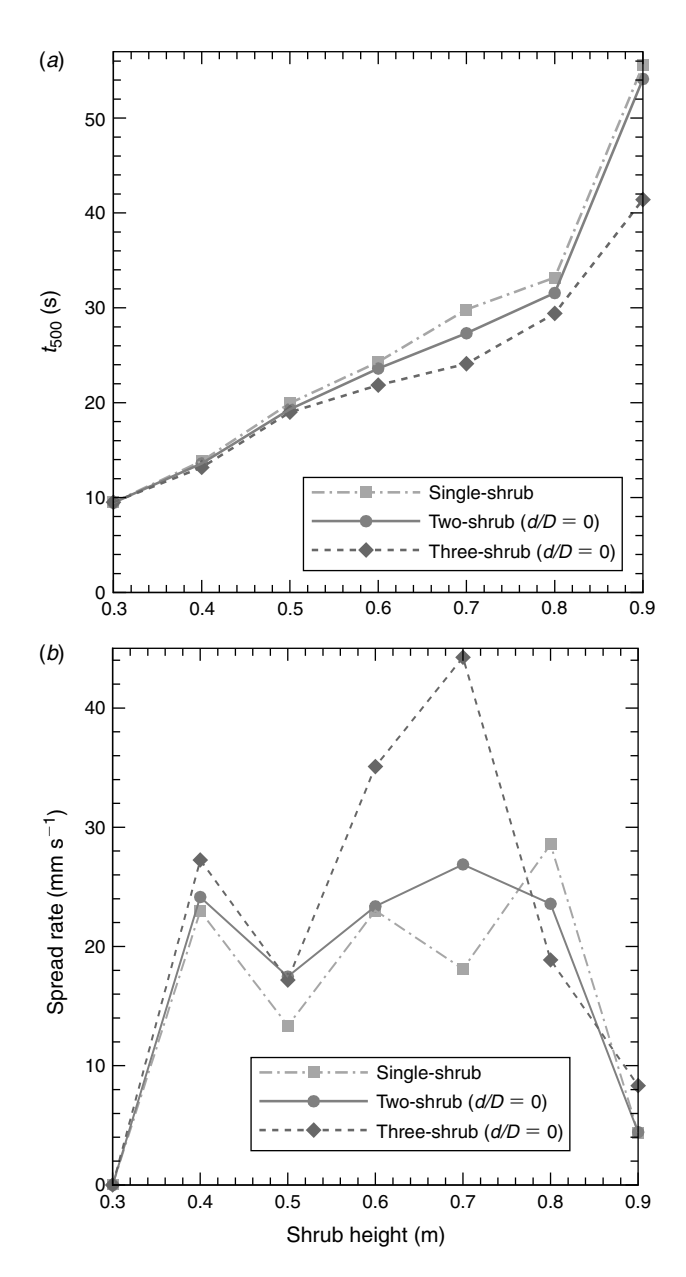


Fig. 12. (a) t_{500} in seconds (time required by the horizontal shrub surface to reach an average temperature of 500 K), and (b) spread rate in millimetres per second as a function of shrub height for single-, two- (d/D=0), and three-shrub (d/D=0) cases respectively. For the two- and three-shrub cases, only one of the shrubs is used to obtain the required data (refer to Fig. 1).

pyrolysis front and is shown in Fig. 12b as a function of the y coordinate. It should be noted that we do not make any assumption such as that fire propagates along the vertical axis of the shrub while deriving or solving the governing equations. It is seen that t_{500} is almost the same for the single-, two- and three-shrub cases for shrub heights below 0.5 m (Fig. 12a), which leads to quite similar spread rates to this height as seen in Fig. 12b. From the shrub height of 0.5 to 0.7 m, the pyrolysis front is seen to move faster in the three-shrub case, the corresponding time interval being between \sim 20 and 30 s. During this time interval, a strong flame-merging phenomenon is observed

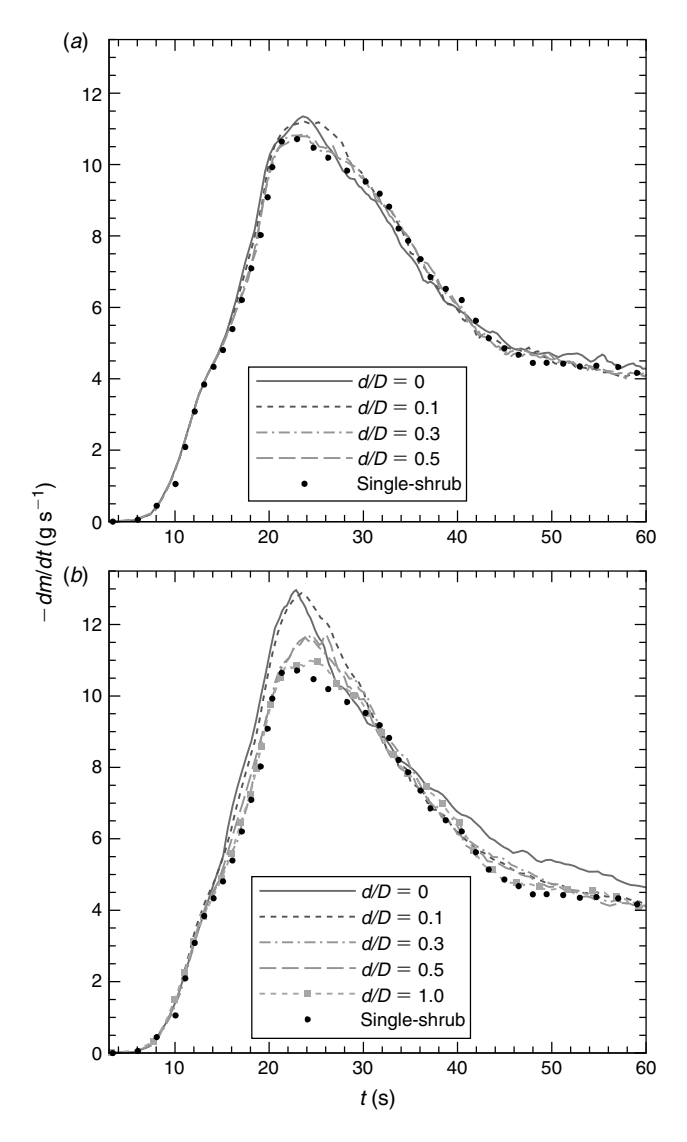


Fig. 13. Time evolution of the mass-loss rate of a shrub in grams per second for (a) two-shrub, and (b) three- shrub cases respectively, with various separation distances (d/D). Mass-loss rate obtained from the single-shrub case is shown with dots.

for the three-shrub case (Fig. 2h), resulting in maximum massloss rate and maximum heat release rate. The spread rates for the two-shrub case are seen to be lower than those for the three-shrub case but higher than for the single-shrub case. This observation suggests a weak flame-merging phenomenon in the two shrub-arrangement.

Non-zero separation

In this subsection, the effect of varying the separation distance between shrubs on the burning of multiple shrubs is examined. Shown in Fig. 13 is the time history of the mass-loss rate per shrub for the two- and three-shrub cases for various separation distances. The time evolution of the mass-loss rate for the single-shrub case is also included in this figure for comparison

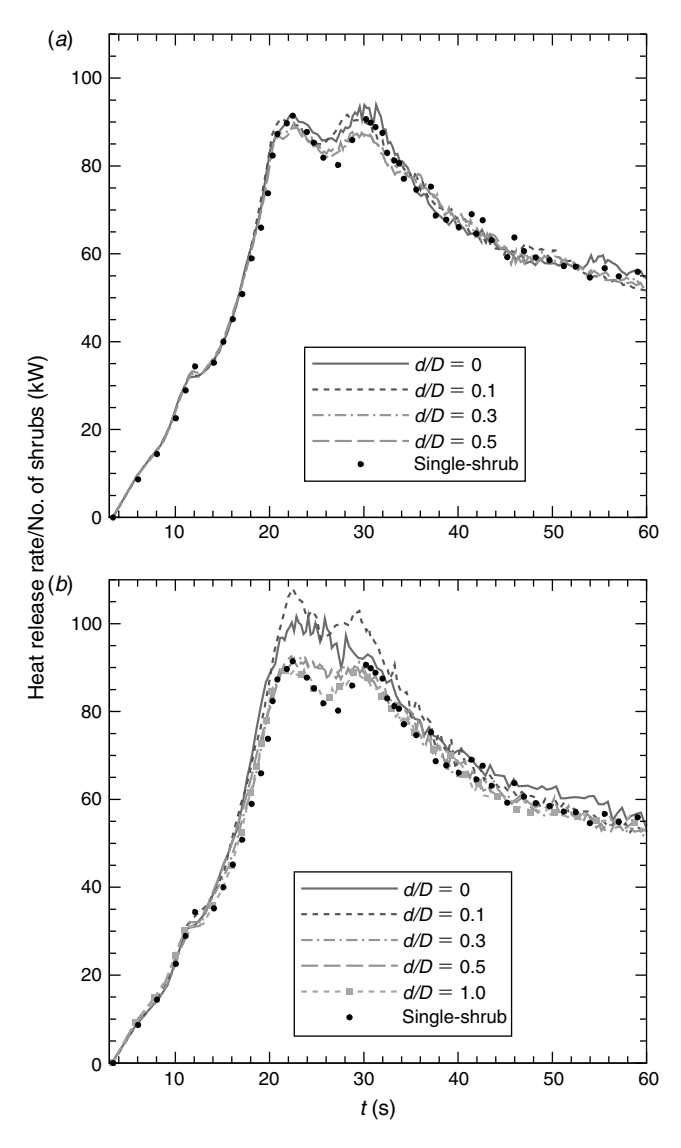


Fig. 14. Time evolution of the heat release rate per shrub in kilowatts for (a) two-shrub, and (b) three-shrub cases respectively, with various separation distances (d/D). Heat release rate obtained from the single-shrub case is shown with dots.

purposes. Although the overall temporal evolution is similar, some deviations are evident in the vicinity of the time of the peak mass-loss rate, which corresponds to the time interval between 20 and 30 s. In both two- and three-shrub arrangements, as the separation increases, the trends of the mass-loss rate become more similar to those in the single-shrub case, indicating a decrease in fire–fire interactions. It is seen in Fig. 13 that the separation distance plays a much more significant role in the evolution of the mass-loss rate in the three-shrub cases.

A similar observation, concerning the effect of shrub separation distance on fire evolution, can be made for the time variation of the heat release rate per shrub, shown in Fig. 14 for various separation distances. When measured with this parameter, the interactions between the individual fires cease to exist at d/D greater than 0.5 for the two-shrub case, as seen in

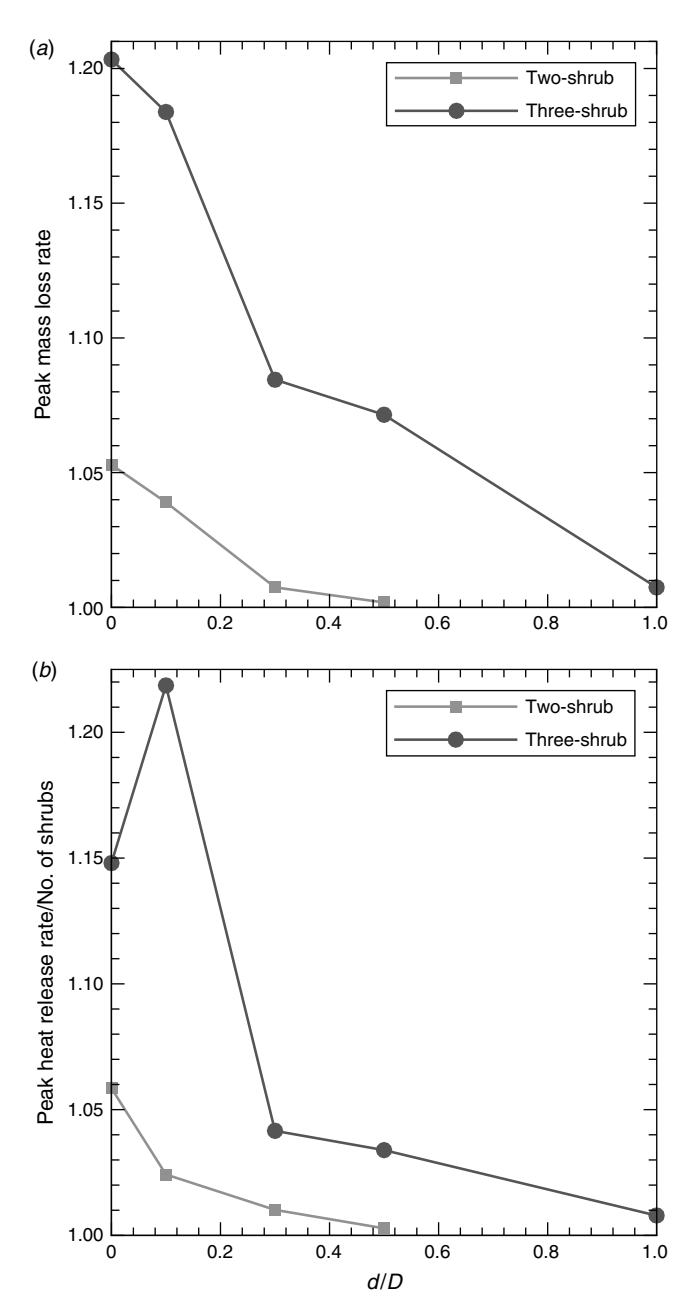


Fig. 15. (a) Peak mass-loss rate for the two- and three-shrub cases normalised by the peak mass-loss rate for the single-shrub case, and (b) peak heat release rate per shrub for the two- and three-shrub cases normalised by the peak heat release rate for the single-shrub case, as a function of crown separation distance (d/D).

Fig. 14a. However, a normalised separation distance of d/D=1 is required to avoid flame merging between the individual shrub fires. Some plume interactions are still seen for the two-shrub case with d/D=0.5 and the three-shrub case with d/D=1 in the far-field region above the shrubs, but these interactions do not impact the burning of the shrubs in any way.

Plotted against d/D for the two- and three-shrub cases are the peak mass-loss rate normalised by the peak mass-loss rate of the single-shrub case in Fig. 15a, and the peak heat release rate per

N Int. J. Wildland Fire A. Dahale et al.

shrub normalised by the peak heat release rate of the single-shrub case in Fig. 15b. It is seen in Fig. 15a that the normalised peak mass-loss rate decreases monotonically with the increase of d/D. At a given d/D, it is substantially larger in the three-shrub case. This parameter converges to nearly unity at d/D = 0.5 for the two-shrub case whereas its convergence to unity is expected to take place at d/D > 1 for the three-shrub cases. The normalised peak heat release rate per shrub, as seen in Fig. 15b, follows a trend similar to that for the normalised mass-loss rate seen in panel (b) except that in the three-shrub arrangement, this parameter experiences an increase at d/D = 0.1. The cause of this phenomenon is explained below.

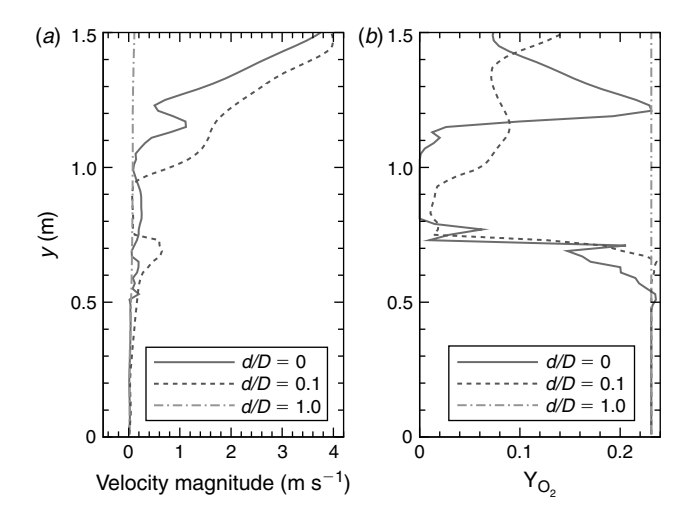


Fig. 16. Spatial variation of (a) velocity magnitude in metres per second; and (b) oxygen mass fraction, along a line passing through the centre of the domain (x=2 m, z=2 m) in the y direction at $t=23\pm0.5 \text{ s}$ (at approximately the time of the peak mass-loss rate), for the three-shrub cases with d/D=0.0, 0.1 and 1.0 respectively.

By analysing the velocity field, it is seen that owing to a small gap between the shrubs for three-shrub case with d/D = 0.1, ambient air is able to enter the region surrounded by the shrubs. Owing to the entrainment of ambient air into the interaction zone, higher velocities and oxygen concentrations are formed at a separation distance of 0.1 for the three-shrub case. Velocity magnitude and O₂ mass fraction are plotted along the vertical centre-line of the domain in Fig. 16a and b, respectively, at the time of the peak mass-loss rate in the three-shrub arrangement. A region with almost negligible oxygen concentration is seen to exist for d/D = 0 near the top surface of the shrub (y = 0.1 m), as seen in Fig. 16b, at the time of the peak mass-loss rate. By comparing similar snapshots at other time instances, the oxygen depletion region was seen to prevail throughout the time interval between 20 and 30 s for d/D = 0. Thus, a smaller heat release rate seen for d/D = 0, as compared with that for d/D = 0.1, could be attributed to the unavailability of oxygen in this region. Also, the cross-stream velocities induced by the gap between the shrubs for d/D = 0.1 result in an increase in vorticity magnitudes through the mechanism of gravitational torque generation, as explained earlier in reference to Fig. 9. This increase leads to an enhanced mixing between pyrolysis gases and oxidiser. Faster combustion, promoted by enhanced mixing of fuel and oxidiser, results in high heat release rates in the case with d/D = 0.1compared with the case with d/D = 0. Furthermore, when d/D = 1, it is seen in Fig. 16 that owing to lack of interaction between neighbouring fires, the velocity magnitude and O₂ mass fraction along the centre-line of the domain behave no differently from ambient conditions.

Finally, the effect of the shrub separation distance on the fire spread rate and the amount of fuel consumed in the vertical direction were investigated. These two parameters are considered important from a prescribed-burning standpoint (Weise *et al.* 2005). Fig. 17*a* shows the average fire spread rate inside the shrub for the two- and the three-shrub cases, normalised by the average fire spread rate obtained for the single-shrub case,

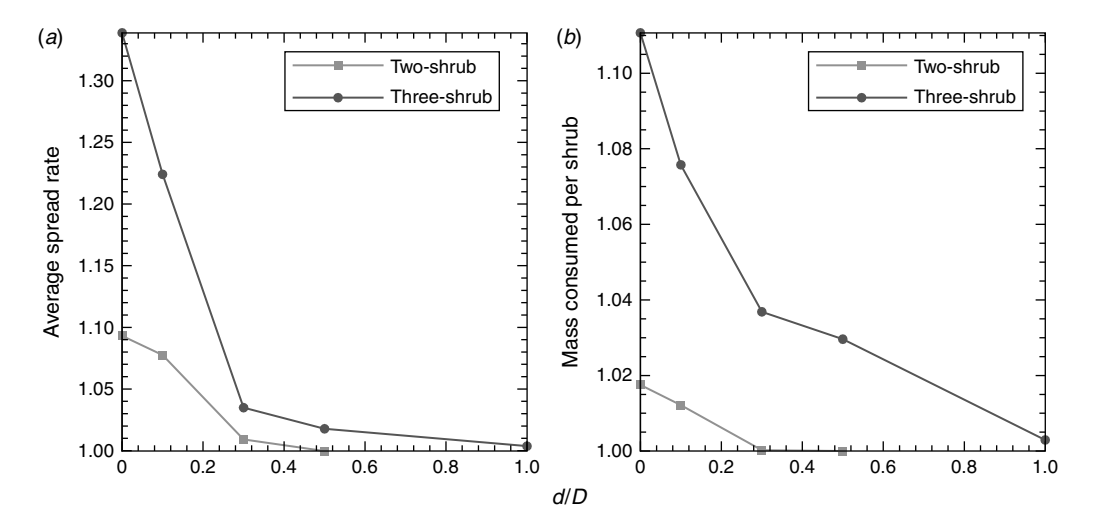


Fig. 17. (a) Average fire spread rate in y direction for the two- and three-shrub cases normalised by the average fire spread rate for the single-shrub case, and (b) the amount of shrub mass consumed in first 60 s for the two- and three-shrub cases normalised by the amount of mass consumed for the single-shrub case in first 60 s, as a function of separation distance (d/D).

plotted against d/D. The average spread rate is calculated by averaging the fire spread rate, based on t_{500} criteria, over various horizontal (xz) shrub surfaces ranging from 0.3 m (base of the shrub) to 0.8 m (approximate height to which the shrub is burned in 60 s). Similarly, Fig. 17b shows the variation in the amount of fuel consumed in 60 s for the two- and the three-shrub cases, normalised by the amount of the fuel consumed for the singleshrub case in 60 s, as a function of d/D. Both parameters, the spread rate and mass of solid fuel consumed, decrease with increasing separation distance. Moreover, as noted earlier, when d/D = 0, the three-shrub configuration generates stronger interactions between individual fires, leading to higher fire spread rates (~1.24 times higher) with an increased mass consumed (\sim 1.16 times higher) as compared with the two-shrub case. For the three-shrub case with d/D = 1 and the two-shrub case with d/D = 0.5, the average spread rate and the mass consumed are equal to that for the single-shrub case, indicating that the neighbouring fires do not impact the solid fuel burning at these separation distances.

Conclusion and future work

Computational modelling of two- and three-shrub fires was performed to study the interaction between shrub fires and its effects on fire behaviour. Two shrubs were placed adjacent to each other in the two-shrub arrangement and three shrubs were placed at the vertices of an equilateral triangle in the three-shrub arrangement. In both arrangements, shrubs were ignited simultaneously with the aid of small ignition zones placed underneath the shrubs. For comparison purposes, an additional set-up consisting of a single isolated shrub (single-shrub case) was also modelled.

When the shrubs were placed next to each other with zero separation distance (d/D=0), flames from individual shrub fires interacted strongly, displaying an almost unified flame for the three-shrub arrangement. Fire–fire interactions, though present, were seen to be much weaker for the two-shrub arrangement. Flame height in the case of two-shrub arrangement was observed to be slightly larger than that of the single-shrub case. However, the flame height in the three-shrub arrangement was observed to be substantially larger than that in the two-shrub arrangement. The buoyancy-driven flow field for the three-shrub arrangement with $d/D \le 0.5$ appeared to be drawn towards the centre of the domain.

The region surrounded by three shrubs in the three-shrub arrangement with $d/D \le 0.1$ was characterised by high magnitudes of vorticity. By evaluating and tracking various source terms in the vorticity transport equation, it was observed that vorticity was mainly generated through the gravitational torque mechanism, which essentially involves a dynamic interaction of the misalignment between the density gradient vector and the gravitational acceleration vector. This mechanism for vorticity generation was found to be much weaker for the two- and single-shrub cases. Higher vorticity generated in the three-shrub cases with $d/D \le 0.1$ led to a faster mixing of pyrolysis gases and surrounding air, which resulted in vigorous gas-phase combustion. This effect was confirmed by analysing the time history of total heat release rate divided by the number of shrubs in the domain. The peak value of this parameter for the three-shrub

case with d/D=0 was found to be 15% higher than for the single-shrub case. Similarly, the peak value of heat release rate per shrub for the two-shrub case with d/D=0 was 5% higher than the single-shrub case. For d/D=0, owing to an enhanced heat feedback from gas to solid phase, the average fire spread rate for the three-shrub case increased by almost 35% and for the two-shrub case by 10%, as compared with that of the single-shrub case. An \sim 20% increase was seen in the peak mass-loss rate value for the three-shrub case with d/D=0 over the single-shrub case. This increase for the two-shrub case with d/D=0 was 5%.

Fire-fire interactions and the corresponding flame merging diminished as the separation between the shrubs was increased. For the two-shrub arrangement with d/D = 0.5, the behaviour of fire was seen to be very similar to that of a single isolated burning shrub, which indicated an absence of interactions between the two fires. For the three-shrub arrangement, a d/ D value of at least unity was required to stop the fire-fire interactions. The peak value of heat release rate per shrub for the three-shrub arrangement with d/D = 0 was found to be \sim 6% lower than that with d/D = 0.1. It is shown that this effect is due to the inability of ambient air to enter the combustion zone, which creates an oxygen-deficient region near the top surface of the shrubs for the three-shrub case with d/D = 0. The peak mass-loss rate, the vertical fire spread rate within the shrub and the mass consumed within the first 60 s decreased with an increase in separation for both two- and three-shrub cases until their respective values were equal to those seen in the single-shrub case.

Quantifying the interactions occurring between the plumes, investigation of merged-flame properties and exploring the effects of spatial distribution of bulk density and moisture content variation on flame-merging phenomena will be the focus of future work. Owing to limited access to experimental facilities, validating simulation results through experiments was not possible. Conducting experiments focussed on shrub fire merging will be an additional direction of future work.

Acknowledgements

The authors are grateful to the National Science Foundation (grant number CBET-1049560) and the 2013 Individual Investigator Distinguished Research (IIDR) program at The University of Alabama in Huntsville (UAH) for providing financial support for this work. Computational resources were provided by the Alabama Supercomputer Center (ASC), the Extreme Science and Engineering Discovery Environment (XSEDE), which is supported by National Science Foundation grant no. OCI-1053575, and the High Performance Technical Computing (HPTC) facilities at UAH.

References

Albini FA (1981) A model for the wind-blown flame from a line fire. *Combustion and Flame* **43**(0), 155–174. doi:10.1016/0010-2180(81) 90014-6

Anderson HE (1969) Heat transfer and fire spread. USDA Forest Service Research, Intermountain Forest and Range Experiment Station, Paper INT-69. (Ogden, UT)

Baldwin R, Thomas PH, Wraight GH (1964) The merging of flames from separate fuel beds. Fire Research Station, Boreham Wood, Fire Research Note No. 551. (Hertfordshire, UK)

P Int. J. Wildland Fire A. Dahale et al.

- Baum HR, McCaffrey BJ (1989) Fire-induced flow field theory and experiment. Fire Safety Science 2, 129–148. doi:10.3801/IAFSS.FSS. 2-129
- Boersma BJ, Brethouwer G, Nieuwstadt FTM (1998) A numerical investigation on the effect of the inflow conditions on the self-similar region of a round jet. *Physics of Fluids* **10**(4), 899–909. doi:10.1063/1.869626
- Byram GM (1954) Atmospheric conditions related to blow-up fires. USDA Forest Service, Southeastern Forest and Range Experiment Station, Paper 35. (Asheville, NC)
- Countryman CM (1964) Mass fires and fire behavior. USDA Forest Service, Forest and Range Experiment Station, Research Paper PSW-19. (Berkeley, CA)
- Dahale A (2014) Dynamics of shrub fires investigated via physics-based modeling. PhD thesis, The University of Alabama in Huntsville.
- Dahale A, Ferguson S, Shotorban B, Mahalingam S (2013) Effects of distribution of bulk density and moisture content on shrub fires. *International Journal of Wildland Fire* 22, 625–641. doi:10.1071/ WF12040
- DesJardin PE, O'Hern TJ, Tieszen SR (2004) Large-eddy simulation and experimental measurements of the near-field of a large turbulent helium plume. *Physics of Fluids* **16**(6), 1866–1883. doi:10.1063/1.1689371
- Finney MA, McAllister SS (2011) A review of fire interactions and mass fires. *Journal of Combustion* **2011**, 1–14. doi:10.1155/2011/548328
- Fukuda Y, Kamikawa D, Hasemi Y, Kagiya K (2004) Flame characteristics of group fires. Fire Science and Technology 23(2), 164–169. doi:10.3210/FST.23.164
- Ghoniem AF, Lakkis I, Soteriou M (1996) Numerical simulation of the dynamics of large fire plumes and the phenomenon of puffing. Symposium (International) on Combustion, 26(1):1531–1539.
- Hunt JCR, Wray A, Moin P (1988) Eddies, stream, and convergence zones in turbulent flows. Center for Turbulence Research Report CTR-S88.
- Kamikawa D, Weng W, Kagiya K, Fukuda Y, Mase R, Hasemi Y (2005) Experimental study of merged flames from multifire sources in propane and wood-crib burners. *Combustion and Flame* 142(1–2), 17–23. doi:10.1016/J.COMBUSTFLAME.2005.02.004
- Li J (2011) Experimental investigation of bulk density and its role in fire behavior in live shrub fuels. MS thesis, University of California Riverside.
- Lozano JS (2011) An investigation of surface and crown fire dynamics in shrub fuels. Phd thesis. University of California Riverside.
- McGrattan KB, Hostikka S, Floyd JE, Baum HR, Rehm RG (2007) Fire Dynamics Simulator (Version 5): technical reference guide. NIST Special Publication 1018–5. (The National Institute of Standards and Technology: Gaithersburg, MD)
- Mell W, Jenkins MA, Gould J, Cheney P (2007) A physics-based approach to modelling grassland fires. *International Journal of Wildland Fire* **16**, 1–22. doi:10.1071/WF06002
- Mell W, Maranghides A, McDermott R, Manzello SL (2009) Numerical simulation and experiments of burning Douglas fir trees. *Combustion* and Flame 156(10), 2023–2041. doi:10.1016/J.COMBUSTFLAME. 2009.06.015
- Morvan D, Dupuy JL (2004) Modeling the propagation of a wildfire through a Mediterranean shrub using a multiphase formulation. *Combustion*

- and Flame 138(3), 199–210. doi:10.1016/J.COMBUSTFLAME.2004.
- Morvan D, Hoffman C, Rego F, Mell W (2011) Numerical simulation of the interaction between two fire fronts in grassland and shrubland. *Fire* Safety Journal 46(8), 469–479. doi:10.1016/J.FIRESAF.2011.07.008
- Morvan D, Meradji S, Mell W (2013) Interaction between head fire and backfire in grasslands. Fire Safety Journal 58(0), 195–203. doi:10.1016/ J.FIRESAF.2013.01.027
- Nelson RM, Butler BW, Weise DR (2012) Entrainment regimes and flame characteristics of wildland fires. *International Journal of Wildland Fire* 21, 127–140.
- Pitsch H, Steiner H (2000) Large-eddy simulation of a turbulent piloted methane/air diffusion flame (Sandia flame D). *Physics of Fluids* 12(10), 2541–2554. doi:10.1063/1.1288493
- Pitts WM (1991) Wind effects on fires. *Progress in Energy and Combustion Science* **17**(2), 83–134. doi:10.1016/0360-1285(91)90017-H
- Porterie B, Morvan D, Loraud JC, Larini M (2000) Firespread through fuel beds: modelling of wind aided fires and included hydrodynamics. *Physics of Fluids* 12, 1762–1782. doi:10.1063/1.870426
- Porterie B, Consalvi J-L, Loraud J-C, Giroud F, Picard C (2007) Dynamics of wildland fires and their impact on structures. *Combustion and Flame* 149(3), 314–328. doi:10.1016/J.COMBUSTFLAME.2006.12.017
- Rothermel RC (1984) Fire behavior considerations of aerial ignition. In 'Prescribed Fire by Aerial Ignition, Proceedings of a Workshop', 30 October–1 November 1984, Missoula, MT. USDA Forest Service, Intermountain Forest Sciences Laboratory. (Missoula, MT)
- Satoh K, Naian L, Qiong L, Yang KT (2007) Numerical and experimental study of merging fires in square arrays. In 'Proceedings of ASME 2007 International Mechanical Engineering Congress and Exposition', 11–15 November 2007, Seattle, WA. pp. 461–472. (New York, NY)
- Satoh K, Liu N, Xie X, Zhou K, Chen H-C, Wu J, Lei J, Lozano J (2011) CFD study of huge oil depot fires – generation of fire merging and fire whirl in (7 × 7) arrayed oil tanks. Fire Safety Science 10, 693–705. doi:10.3801/IAFSS.FSS.10-693
- Tachajapong W (2008) Understanding crown fire initiation via experimental and computational modelling. PhD thesis, University of California Riverside.
- Weise D, Zhou X, Sun L, Mahalingam S (2005) Fire spread in chaparral 'go or no-go'? *International Journal of Wildland Fire* 14, 99–106. doi:10.1071/WF04049
- Weng WG, Kamikawa D, Fukuda Y, Hasemi Y, Kagiya K (2004) Study on flame height of merged flame from multiple fire sources. *Combustion Science and Technology* 176(12), 2105–2123. doi:10.1080/00102200490514949
- Zhou X, Mahalingam S, Weise D (2005) Modelling of marginal burning state of fire spread in live chaparral shrub fuel bed. *Combustion and Flame* 143, 183–198. doi:10.1016/J.COMBUSTFLAME.2005.05.013
- Zhou X, Mahalingam S, Weise D (2007) Experimental study and large-eddy simulation of effect of terrain slope on marginal burning in shrub fuel beds. *Proceedings of the Combustion Institute* 31(2), 2547–2555. doi:10.1016/J.PROCI.2006.07.222